WIND ENERGY
Wind Energ. (2010)
Published online in Wiley Online Library (wileyonlinelibrary.com). DOI: 10.1002/we.424

RESEARCH ARTICLE

Design of a scaled wind turbine with a smart rotor for dynamic load control experiments

A. W. Hulskamp[1], J. W. van Wingerden[2], T. Barlas[1], H. Champliaud[3], G. A. M. van Kuik[1], H. E. N. Bersee[1] and M. Verhaegen[2]

[1] Faculty of Aerospace Engineering, Delft University of Technology, Delft, The Netherlands
[2] Faculty of Mechanical Engineering, Delft University of Technology, Delft, The Netherlands
[3] Mechanical Engineering Department, Ecole de Technologie Superieure, Montreal, Canada

ABSTRACT

The ever increasing size of wind turbines poses a number of design issues for the industry, like increasing component mass and fatigue loads. An interesting concept for reducing fatigue loads is the implementation of spanwise distributed devices to control the aerodynamic loading along the span of the blade, thus mitigating fluctuations in loading and adding damping to the blade modes. This is usually referred to as the smart rotor concept. In the design of such a rotor, as compared to a traditional one, the integration of sensors and actuators poses additional design challenges. In the research discussed in this paper, a scaled smart rotor was designed and constructed to study its fatigue load reduction potential. A 1.8 m diameter rotor was manufactured and equipped with trailing-edge flaps. The flaps were based on piezo electric Thunder actuators that allow for high-frequent actuation. The dynamic strain behaviour of the blade was analysed for optimal placement of the sensors. Several sensors that record the strains and accelerations at different locations along the blade were implemented, but the controller was based on a piezo electric strain sensor. The rotor blades were mounted on a small turbine in the Delft University's Open Jet Facility wind tunnel and a mathematical state space model was obtained by using dedicated system identification techniques. Single-Input Single-Output, Multi-Input Multi-Output $\mathcal{H}_\infty$ feedback and feedforward controllers were designed, each focusing on different parts of the load spectrum. The rotor was tested at 0 and 5° yaw angles, with and without load control. A significant reduction of the dynamic loads was attained.

KEYWORDS
smart rotor blades; rotating experiments; fatigue load reduction

Correspondence
A. W. Hulskamp, Faculty of Aerospace Engineering, Delft University of Technology, Delft, The Netherlands.
E-mail: a.w.hulskamp@tudelft.nl

Received 28 January 2010; Revised 3 July 2010; Accepted 4 July 2010

1. INTRODUCTION

Currently, horizontal axis wind turbine (HAWT) manufacturers are facing several challenges related to both a fast increase in turbine size and market growth. The trends force manufacturers to rapidly increase production capacity and to upscale existing blade designs. However, the boundaries of current technologies are being approached. The increase in size is driven by the fact that the power conversion by a wind turbine increases with the square of the rotor's diameter. However, component costs will also increase. For instance, historically, the mass of blades has increased with the radius to the power 2.4[1] to 2.65,[2] depending on how the trend line is fitted. Thus, the mass, and with it the costs regarding materials and installation of a blade, increased faster than the power it captures. This is more acceptable for off-shore turbines than for their on-shore counterparts because a large part of the costs, such as foundations, is related to the number of turbines. Increasing the yield per turbine will, therefore, decrease the costs per kilowatt-hour.

For large turbines, one of the biggest design drivers is fatigue. This is because on top of the mean aerodynamic load, there are several disturbances that cause dynamic deflections of the blade and, thus, fluctuations in the stress distribution. Blades are dimensioned for at least 10^8 cycles. These disturbances are the result of both spatial and temporal changes in

the air speed and direction that the rotor experiences. The causes of these changes are, i.e. wind shear, yaw misalignment, tower shadow and turbulence in the wind. Thus, with ever increasing turbine size, mass effects will also play a larger role. It also adds to fatigue because of the blades' rotation with respect to the gravitational field. Fluctuations in aerodynamic loading will also increase with increasing size, for instance through the more severe wind shear experienced by large machines. In the future, rotors on very large machines might also be mounted downwind, eliminating the tower clearance issue, but increasing the tower shadow effects.

Mitigating the amplitude of the fatigue loads could, therefore, lead to a longer service life of blades, but also possibly to lighter blades. Some features are already applied to control the loads on wind turbines. Passive systems like stall control have been in use for a while. Today, most large turbines are installed with the possibility to control their rotational speed to operate at optimal Tip Speed Ratios (TSRs) at wind speeds below the rated wind speed and pitch control to alleviate loads above rated wind speeds.[3,4] Individual Pitch Control (IPC)[5–7] also has the potential to mitigate fatigue loads, but continuous pitching puts a heavy strain on hydraulics and bearings.

Also, a passive concept, called bend-twist coupling, exists. In this concept, the unidirectional (UD) laminate in the main bending load carrying spar caps is placed at an angle to the blade's longitudinal axis. This way, as the blade bends, it will twist, changing the angle of attack.[8–10] However, the concept is passive and it requires very accurate fibre placement and the implementation of expensive carbon fibres to be successful.

Therefore, the following new concept is proposed: by controlling the aerodynamics at different stations along the blade's span, by e.g. trailing edge flaps, the way the blade is loaded can be controlled, counter-acting the disturbances and mitigating fatigue loads. This, in combination with appropriate sensors that measure the loads or deformations and a controller that computes an actuation signal, is defined as the 'smart' rotor concept. Such an aerodynamic load control system has been intensively investigated for helicopter blades, and feasibility studies for wind turbine blades have also been made recently.[11–19] The goals of the system would be to react both to deterministic loads, such as wind shear and tower shadow, as to stochastic loads such as gusts.

Previous research on the concept mainly focuses on aero-elastic simulations or experiments on 2D sections,[20] In experiments that were conducted prior to this research,[21] the blade dynamics were also taken into account, but the blade was still clamped to the tunnel wall and the disturbances were induced by a predefined pitch motion. In the research described in this paper, a scaled smart rotor was constructed and operated in a wind tunnel to investigate the load alleviation potential of the concept, taking into account the dynamics of the blade and rotationally induced disturbances. This paper will focus on the design of the system and its performance with regard to its potential for load reduction. The main contribution of this paper to the smart rotor research is to expound the design procedure of smart rotor blade design, as well as showing the feasibility of the concept on a rotating set-up.

2. DESIGN AND MANUFACTURING OF AN AERO-ELASTICALLY TAILORED BLADE

In order to investigate the load reduction potential of the concept, a scaled rotor was built on which to perform load reduction experiments in the TU Delft's Open Jet Facility (OJF) wind tunnel. In this section, we discuss the design of the different components of the blades, which include the design of the base structure of the blade, the actuators and the sensor array.

An important issue in the design of the system was the load spectrum that was under consideration. In this case, the rotor did not only have to be scaled with respect to the size and operational settings, but also to the dynamics of the blade.

A turbine is subjected to several disturbances, most of which are related to the rotation of the rotor through a wind field with spatial variations. Thus, they occur with the rotational frequency of the rotor. Examples of these variations are tower shadow and wind shear. Due to sampling of these 1P (once per rotation) disturbances and because multiple blades are mounted to one hub, the blades also experience multiple P loads. The interaction between the first flapwise bending mode and these multiple P excitation loads is an important aspect in the control of the rotor and for the reduction of fatigue loads. After all, disturbances for which the frequency is close to a natural mode excite the blade more severely, as compared to low frequency, quasi-static disturbances. This should be incorporated in the scaled experiment.

Summarizing, the load spectrum and dynamic behaviour of the scaled turbine should reflect that of the full-scale reference design. This was achieved by scaling the first flapwise bending mode frequency of the blades with the rated rotational frequency of the turbine:

$$\frac{f_{model}}{\omega_{model}} = \frac{f_{ref}}{\omega_{ref}} \rightarrow f_{model} = \frac{f_{ref}\omega_{model}}{\omega_{ref}} \tag{1}$$

in which f relates to the frequency of the first flapwise bending mode and ω to the rotational frequency. The subscript *ref* refers to the 5 MW UpWind reference turbine and *model* to the scaled model. See Table I for the operational and design

Table I. Operational parameters that are used for scaling and the aerodynamic design.

	Reference turbine	Scaled turbine
Rated rotational speed (rpm)	12.1	430
Rated wind speed ($m\,s^{-1}$)	11.4	10
Rotor diameter (m)	60	1.8
Design TSR (–)	7	5
First flapwise bending mode (Hz)	0.68	24

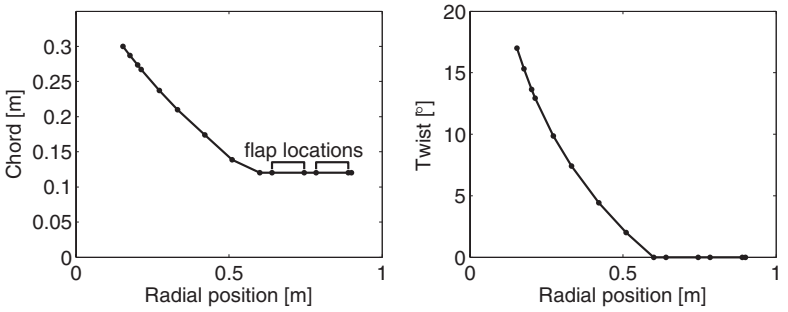

Figure 1. Twist and chord distribution of the blade.

parameters that were used in scaling. The rotational speed of the rotor was set to 7 Hz, which set the target for the first bending mode to 24 Hz. Reynolds scaling was not used, nor scaling to the reduced frequencies.

2.1. Aerodynamic design

The aerodynamic design was based on the operational parameters, with keeping the structure and the actuator design in mind. The design parameters that determined the shape were the twist and chord distribution along the span and the shape of the profile at different radial stations.

The profile shapes along the length of the blade, which determined the absolute thickness of the blade, were initially left open to be determined in the structural optimization process because these had a large influence on the stiffness of the blade. However, after some iteration, we determined that a slender DU96-W180 profile along the whole span of the blade was needed in order to obtain the desired structural properties, i.e. a relative low frequency for the first eigenmode.

The twist and chord distribution were primarily based on the aerodynamic performance of the turbine and derived using a Blade Element Method (BEM)-based optimizer. In this optimization procedure, a restriction was formed by the installation of the actuators. To successfully implement the actuators in the tip, a straight tip—without twist and taper—was desired. A chord of 12 cm was chosen for this section. These specific dimensions were chosen because of experiences obtained in previous experiments.[21,22] Here, it led to a tip Reynolds number of $2.4{\cdot}10^5$, which was much lower than the reference turbine. However, as mentioned before, we were not trying to use Reynolds scaling in this work. For the performance of the aerofoil sections with actuators, XFOIL[23] calculations were performed on the adapted aerofoil shape (also see 'Actuator design' below). The calculations were corrected for rotational effects.[24]

With these requirements and the turbines operational settings in mind, the aerodynamic design could be optimized. Due to the restrictions mentioned above, attaining an aerodynamically optimal design turned out to be impossible. However, obtaining an optimally performing turbine was not the goal of this project, so the design was adapted to fit the shape requirements. Moreover, the predicted loading was enough to drive the turbine and provide an observable and distinctive sensor signal. The derived twist and chord distribution can be seen in Figure 1.

2.2. Structural design

2.2.1. Conceptual design

The blades were designed to be of a glass–epoxy laminate, which was infused in a double rigid mould, after being wrapped around a solid foam core. Thereby, the gap between the mould surface and the foam core was filled with resin and the preform was infused. Through this process, a strong but flexible blade with a smooth outer surface could be

obtained. The glass reinforcement was a S303 8H-satin weave (Ten Cate Advanced Composites, Nijverdal, The Netherlands), which was used for its fine tows and good drapability. The resin used was an Epikote 04908 resin with an Epikure 04908 hardener (Hexion, Rotterdam, The Netherlands). This is a resin that is used in the wind turbine industry, but it was specifically used here for its long pot life, which was needed for infusion. The chosen foam was a 200 kg/m^3 Airex C70.200 (Airex AG, Sins, Switzerland). This high-density foam was chosen because it allowed for high accuracy milling and because it provided good support for the skin.

The foam core was fitted with a steel foot, which was used to mount the blade to the hub. Two 5 mm holes were drilled through the foam, one on and the other just behind the pitch axis along the length of the blade. One hole was used to fit the sensor and actuator cables and the other to fit a safety cable. The straight outboard section was equipped with a glass-epoxy spar. The spar was prefabricated and assembled with the foam core and steel inserts before infusion of the skin. The spar acted as mounting point and reinforcement where the actuator slots were cut out after resin infusion of the skin. It consisted of eight plies of the same glass-reinforcement and epoxy materials as the skin.

2.2.2. Laminate detailing

The laminate lay-up was used to tune the blade dynamics, stiffness and strength to the desired values. As mentioned, a target eigenfrequency of 24 Hz for the flapwise bending mode was the goal. This meant that quite a flexible blade had to be attained. However, strength and buckling requirements also had to be met at the same time. The blade was analysed using a finite element (FE) model in Ansys. The FE model consisted of quadratic shell for the skin and solid elements for the steel and foam core. The material properties were obtained from manufacturers' data or from previous experiments.[25] The properties of the laminate were adjusted for a lower fibre volume fraction V_f using micromechanical modelling. V_f was relatively low because the fabrication process leads to a lower compaction of the glass weave.

Several analyses were performed with the FE model. Firstly, a static analysis was performed to analyse the strength of the blade. The loads for the analysis were obtained from the BEM analysis. To evaluate laminate strength, a maximum strength criterion was implemented and Plantema's theorem was used to evaluate for skin wrinkling.[26] An iterative design procedure proved that with a laminate thickness of 0.5 mm, the stresses stayed within the allowable stresses and skin wrinkling would not occur. A linear modal analysis predicted a first flapwise bending mode frequency of 33 Hz, which was higher than the target frequency of 24 Hz, but linear modal analyses typically overestimate eigenfrequencies. Moreover, the blade mounting to the hub was more flexible than modelled.

2.3. Actuator design

Camber control was achieved by sawing slots at two locations in the blade's straight outboard section, as indicated in Figure 1. The outer slot was placed as far outboard as possible in order to have as large an effect as possible on the root bending moment when actuating the flap. The second slot was placed as far inboard on the straight section as possible so the actuators can also control higher modes, which would require exerting a moment at the tip by opposite flap motion. But here we focused on the first bending mode. The slots were fitted with the actuators. These so called Thunder (Face International Corporation, Norfolk, VA)[27] actuators were placed in line with the suction side of the aerodynamic profile (see Figure 2).

The actuators are much larger in chordwise sense than would be needed on full scale blades, but here they were implemented as 60% of the chord for the purpose of producibility of the flaps and flap authority. The curvature of the actuators coincided fairly well with the curvature of the profile (see Figure 3). Placing the actuators here would assure a smooth and solid surface on the suction side. This was needed for more predictable performance of the actuator and to have a qualitative good boundary layer over the actuator. Previous experience with placing the Thunder in the centre and match-

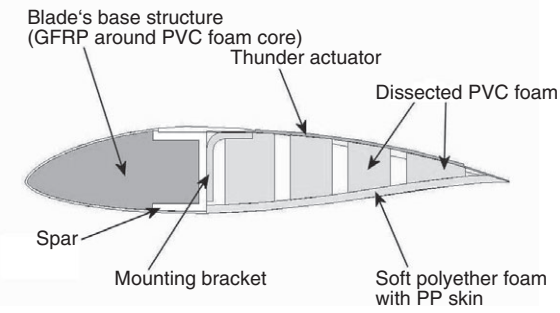

Figure 2. Design of the morphing camber control surface.

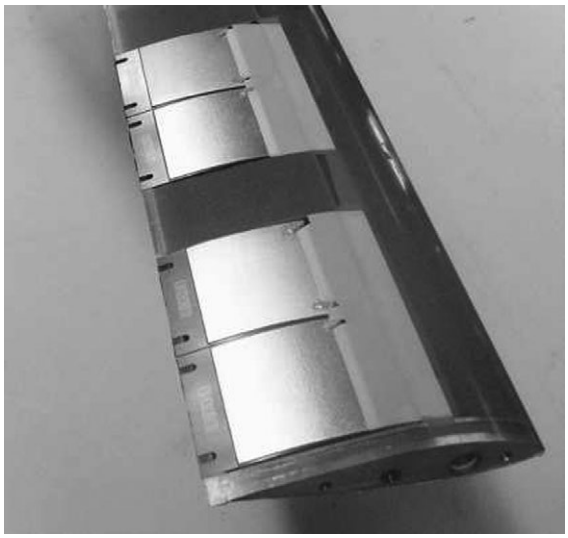

Figure 3. Installed Thunder actuators, suction side view.

ing the shape of both the pressure and suction side with foam that was covered with an elastomeric skin gave unsatisfactory results. Here, the slight mismatch in surface curvature between the baseline profile and actuator surface was considered acceptable.

The remainder of the shape of the aft part of the profile was achieved by filling the slot with foam and covering it with a polypropylene (PP) film. Two types of foam were implemented: dissected rigid foam filled the largest part of the space; this was covered with a soft polyether foam patch to smoothen the sections of the rigid foam (see Figure 2). The rigid foam was implemented to prevent the suction side from denting under the aerodynamic pressure, which was also observed in the previous experiments. The Thunder actuators were attached to the blade by means of an aluminium bracket to which it was adhered. This method of mounting increased the first eigenfrequency of the bender to about 90 Hz, compared to the 40 Hz that was observed when using a bolted connection. A weak part of the actuator design is still the flexible skin on the pressure side. Predictions on flap performance were based on XFOIL calculations for rigid flaps. The shape of the profile was obtained using measurements of the actuator shape and deflections. It was, though, quite hard to estimate actual flap angles.

2.4. Blade and sensor testing

A different set of experiments was conducted to evaluate the blade's behaviour and the sensor performance. Three strain sensors were evaluated; strain gauge, PVDF-patches[28] and MFCs (Smart Material Corp., Sarasota, FL).[29] The blade was subjected to several dry tests outside the wind tunnel to test the sensor performance and to validate the FE model. Firstly, the blade was excited at the outboard section by a sinusoid signal and the sensor signals were recorded.

All sensors seemed to capture the excitation signal well, although with different signal to noise ratio's. In addition, a free vibration test was performed. From the different tests, conclusions about the performance of the different sensors can be drawn. In Figure 4, the response of different sensor signals to a transient vibration can be seen.

The magnitude of the sensor signals could be amplified, but several conclusions can be drawn about the quality of the signal. First of all, the PVDF film showed a clear spike at 50 Hz. Because of its low capacitance it easily picked up electro magnetic interference. The MFC signal followed the behaviour of the captured strain well. Actually, the MFCs proved to give the best signal and, in contrast to strain gauge, the signal required no amplifier. However, because of their high impedance they are quite susceptible to electromagnetic noise, but not as severe as the PVDF. Here, proper shielding and filtering mitigated the noise. The electrodes of the MFC were bridged by a resistor and a capacitor. This way, a sensor with a high-pass filter was obtained effectively. Two MFCs were adhered to each blade—one on the pitch axis to measure normal stresses that arose from a flapwise bending moment and one on the leading edge to measure the strains associated with an edgewise bending moment. The optimal location was determined using a harmonic analysis. From this analysis, the amplitude and phase of stress and strain in the blade in response to an excitation load was derived. Using this analysis a sensor location on the blade that would provide a high stress amplitude and good phase behaviour was determined.

Finally, a static experiment was performed and only 4% deviation in stiffness between the FE model and the test blade was observed.

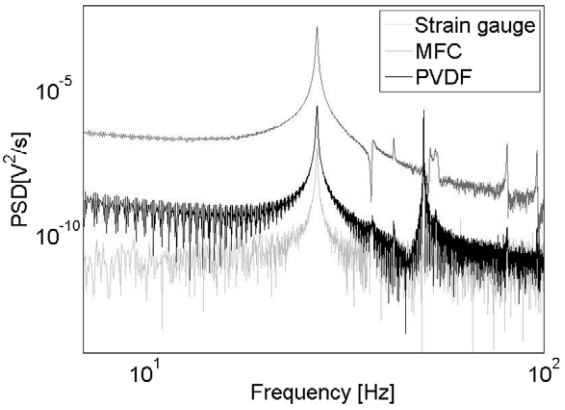

Figure 4. PSD of the sensor signals to a transient load.

3. WIND TUNNEL SET-UP

In this section the set-up in the wind tunnel is discussed, which includes the specifications of the tunnel itself, an overview of the whole system and the design of the controller. The controller was based on a measured state space model of the turbine, using system identification techniques. Thus, the controller was designed and tuned using data obtained from experiments on the blades mounted on the turbine.

3.1. Wind tunnel and turbine

3.1.1. Wind tunnel

The experiments were conducted in the OJF wind tunnel.[30] This tunnel has a closed circuit with an open test section. The air travels through the circuit in the following manner. Starting just before the rotor plane, it enters the test section through an octagonal nozzle, creating a steady jet with an effective diameter of 3 m. There are little or no wall effects because the section is 6 m wide and 6.5 m high; much larger than the jet (see Figure 5).

The air is collected at the back of the test section, cooled and fed back into the tunnel's fan after the flow direction is reversed around two 90° corners with a series of corner vanes. After the fan, the flow direction is again reversed around

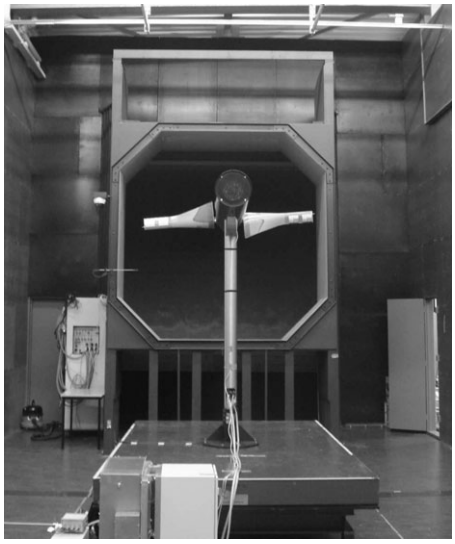

Figure 5. The turbine in the test section, with the rotor in the jet. Picture was taken in the direction opposite to the airflow.

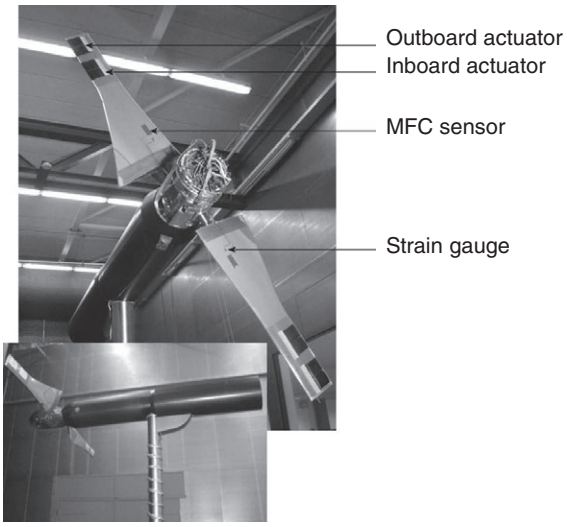

Figure 6. Wind tunnel set-up for load alleviation experiments. At the bottom the fully installed turbine can be seen. The air flows from left to right.

a set of corner vanes. Before it is blown through the nozzle back into the test section, it enters a settling chamber with several rows of wire meshes to reduce the turbulence levels. The tunnel's fan is powered by a 500 kW motor with which a maximum air speed of 35 m s^{-1} in the jet is attainable.

3.1.2. Generator control and the nacelle

The blades were mounted to a small turbine in the wind tunnel, see Figure 6. The turbine is designed specifically for model tests in the OJF. Its generator is actually a synchronous AC servo motor, with a maximum power of 5 kW. If the turbine works as a wind energy conversion system (WECS) and the shaft torque is negative, then the motor works as a generator and electric power is dissipated by a dissipator.

Feedback of the rotor speed and position is done through an encoder. The rotor plane is 1 m upwind of the tower so the blades experience no tower shadow. The conical hub is mounted to a shaft that runs along the whole length of the nacelle. The front end of the nacelle between the hub and the generator, which is installed on top of the tower, only contains the drive shaft. The aft section contains the slip rings that transferred signals from and to the fixed world. The hub has a diameter of about 30 cm. The tower has a diameter of about 15 cm and a helical cable is wound around the tower (see Figure 6) to suppress flow separation and tower vibrations resulting from that. The turbine's controller is programmed through a LabVIEW system (National Instruments Netherlands BV, Woerden, The Netherlands), which acts as a graphical user interface (GUI). The actual operational parameters, such as generator speed and torque, are also fed into this LabVIEW system to be displayed on screen for monitoring purposes. In the experiments discussed here, the control of the generator was set to speed control.

3.1.3. Rotor control system

All actuator and sensor cables of the blades were connected according to the scheme in Figure 7. The signals were fed through the hub and then transferred over slip rings to and from the fixed world. The hub was also powered by a 7 V DC voltage. This was used to power the accelerometers in the blades and the strain gauge amplifiers. The signals of the MFCs were transferred unamplified. The actuation signal for the flaps was amplified on the ground and then transferred to the blades over the slip rings.

The controller for the flaps was designed and programmed in a Matlab and Simulink (The MathWorks, BV, Gouda, The Netherlands) environment and compiled to the dSPACE real time control system (dSPACE GmbH, Paderborn, Germany). Commands, such as manual flap control and controller gains, could be altered in the ControlDesk GUI. Moreover, the measurement signals were also plotted in ControlDesk and recorded on the hard disk. All signals to and from the blade as depicted in Figure 7 were transferred to the hub in two fold; one set for each blade.

As can be seen in Figure 7, the turbine and rotor control systems were fully separated, except for the recording of the azimuthal trigger. The only task of the LabVIEW-controlled system was to maintain constant rotor speed. The dSPACE system, on the other hand, was only concerned with the loads on the rotor blades. It had no control over the rotor speed

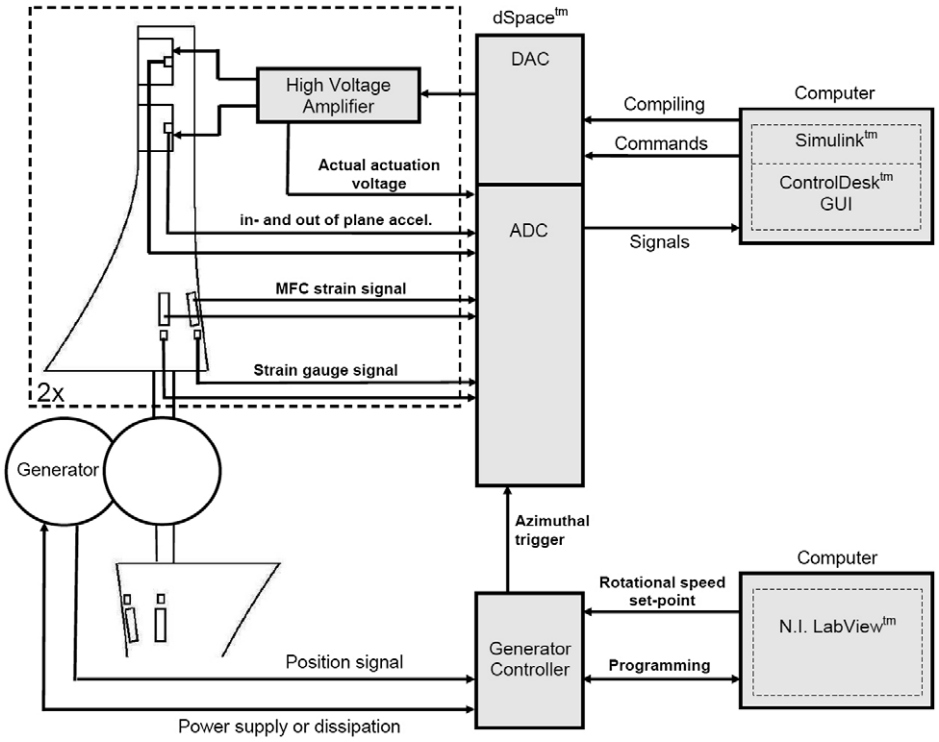

Figure 7. Control scheme of the smart rotor.

or torque. The two systems were separated in order to have constant operational conditions of the turbine when the rotor was subjected to different external fluctuations.

3.2. Operational conditions

A series of experiments was performed. Here we focus on the results of the rotor in yaw. 0 and 5° yaw were tested. The no-yaw condition was tested as a baseline, but this case already posed a significant load case, as we will see later. The rotational speed was set to 370 rpm, although the rated rotational speed is 430 rpm. This had to be done, because of problems with controlling the rotor speed at high rpm. Although the rotational speed in the experiments presented here was not the rated speed, a similar interaction between rotationally induced disturbances and the first flapwise bending mode was kept because the 4P loads were still close to the first flapwise bending mode (see Figure 8). The wind speed was changed to 7 m s^{-1}. This resulted in a slightly higher TSR than as designed. This was done in order to increase the power conversion.

The exact operation point of the turbine, in terms of thrust and power coefficient, was hard to determine because the thrust and torque measurement capability of the turbine was not available when the tests were performed.

3.3. Controller design

A dynamic state space model was obtained through system identification.[31] The system's inputs were the control signals to the high-voltage amplifiers that drove the Thunder actuators and the system's outputs consisted of the MFC sensor signals. The flaps were given a GBN-noise signal, a block signal with a fixed amplitude and a certain bandwidth, and the response of the blade was measured through the MFCs. In all experiments reported here, the in- and outboard flap were being controlled by the same actuation signal, as depicted in Figure 7. This effectively reduced both flaps to one flap, but in future experiments, the flaps can be operated individually. The results can be seen in Figure 9. This figure displays the transfer from a signal to the flaps on the respective blades, to the strain signal on both blades, as a function of the actuation frequency. There was a considerable amount of coupling, indicated by the high values for the transfer between flap actuation on one blade to the sensor on the other (see the top-right and bottom-left graphs in Figure 9).

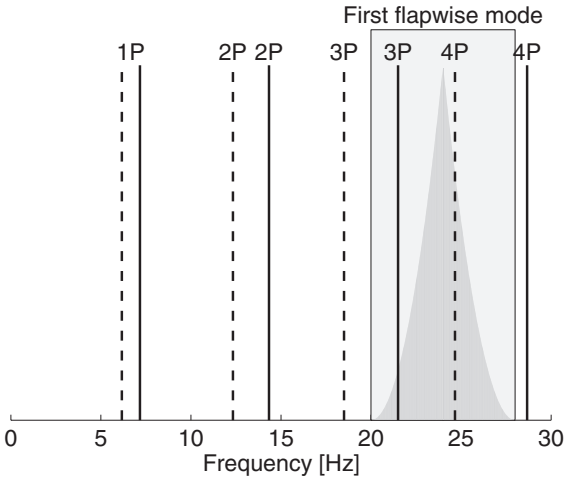

Figure 8. Interaction between the rotational frequency and the blade's first eigenmode. The dashed lines mark 370 rpm and the solid lines 430 rpm. The frequency range over which there was an interaction between the multiple-P loads and the first flapwise bending mode, is indicated as the light-grey area. In this, the resonance peak is schematically represented in grey, with its peak at 24 Hz.

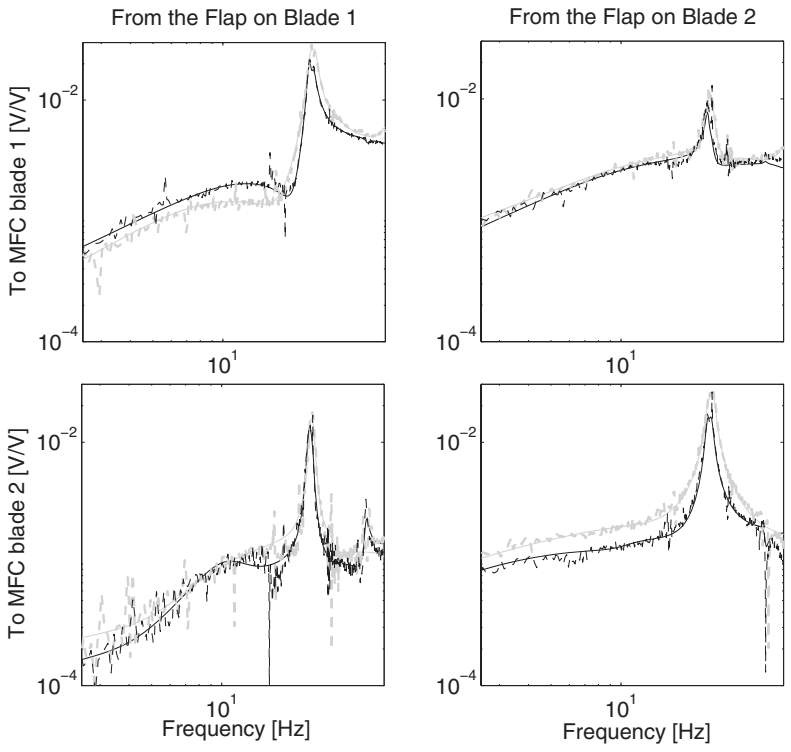

Figure 9. Bode plots of the measured flap actuation to blade load measurements and the fitted state space model. Grey depicts the model for 420 rpm and black for 370 rpm. The dashed lines represent the measurement data and the solid lines the obtained model.

Several controllers were designed using this state space model. Firstly, a Single Input, Single Output (SISO) PID controller, similar to those used in previous experiments[21] was implemented. Two SISO controllers, one for each blade, worked parallel to each other, but the two gains were tuned successively. The controllers took their input signal from the MFC on each respective blade and provided a single actuation signal for both flaps on that same blade. Secondly, a $\mathcal{H}_\infty$ Multiple Input Multiple Output (MIMO) feedback controller with the same in and outputs was designed with a combination of notches at 1, 2, 3 and 4P loads, as well as added damping to the first flapwise bending mode.

In addition, the potential of feedforward control was investigated. The controller was tuned by Repetitive Control (RC)[32] scheme. Because it is less common, its implementation requires some explanation. RC is a form of feedforward control and can be applied to systems which are excited by the same disturbance over and over again. This is clearly the case for rotating turbines. With RC, the error signal over a certain cycle, called a trial, is captured and after each trial the controller parameters are updated. Moreover, the number of parameters that is to be tuned can be reduced by selecting a certain set of base functions, resulting in a so-called structured feedforward signal. Here, we chose a sine and cosine function with a frequency that was equal to the rotational speed of the turbine because we were trying to reduce the 1P loads:

$$u_k^{(ff)} = \theta_k^s \sin(\omega t) + \theta_k^c \sin n(\omega t) \tag{2}$$

In equation (2), θ_k^s and θ_k^c are the parameters to be tuned and that are updated every trial, ω is the rotational speed of the turbine and the subscript k denotes the k^{th} trial. The technique was attractive because an accurate dynamic model of the system was not needed. A scheme for the feedforward controller, including a feedback controller, can be seen in Figure 10.

Both the feedforward and the feedback controller acted on the error signal and provided an actuation signal, but the feedforward controller provided a preselected signal—here the sum of a sine and cosine function—for which the gains were tuned by an update law. The timer was added in Figure 10 to the update law to indicate that the update law was not a continuous process, but was executed once every trial. On the smart rotor turbine, the timer was implemented in the form of the azimuthal trigger that generated a pulse when the rotor was in a certain azimuthal position. This way, small errors in rotational speed did not disturb the update process, as would be the case when the update law had been executed every assumed time period.

The challenge was to tune θ^s and θ^c. This was done by minimizing an objective function V:

$$\min_{\theta_k} = V(\theta_k)$$

in which: $\theta = [\theta^s\ \theta^c]$. The objective function was chosen to be the square of the 2-norm of the error signal over the k^{th} trial e_k:

$$V(\theta_k) = e_k^T(\theta_k) e_k(\theta_k) \tag{3}$$

A trial in this case was one time series over the repetitive period; in our case one revolution. The error was equal to the output (the MFC signal) since the set point was zero for all t. We did not have to compensate for the static load because

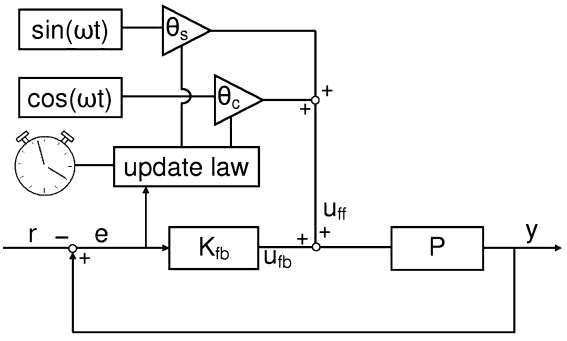

Figure 10. Scheme for feedforward control, including a feedback controller. P denotes the plant and K_{fb} the feedback controller.

the MFC did not capture this. The optimization algorithm used Newton's method to which a forgetting factor β was added. This led to:

$$\theta_{k+1} = \beta\theta_k - \alpha L_k e(\theta_k) \tag{4}$$

α is the learning factor. L was derived off-line from the system identification data. See van der Meulen *et al.*[32] for details.

4. RESULTS

In this section, we will present the results obtained with the setup and the different controllers as discussed above. Three cases are discussed. First, the load reduction attained with two uncoupled SISO controllers will be shown. Secondly, we will show the results of the MIMO controller and finally, the load reduction attained by the MIMO controller, in combination with adaptive feed forward control on the 1P loads will be presented. An overview of the load cases and the different controllers used in those respective cases are depicted in Table II.

4.1. SISO control

The results obtained with the SISO controllers for different yaw angles can be seen in Figures 11 and 12. In these spectra plots, the 1, 2, 3 and 4P load spikes, as well as the resonance peak at 24 Hz—as designed—are clearly visible. Also, the

Table II. Different load cases with controller types.

Controller configuration	Controller type	Case 1	Case 2	Case 3
SISO	PD with notch filter	X		
MIMO	$\mathcal{H}_\infty$		X	X
Feedforward	Repetitive control			X

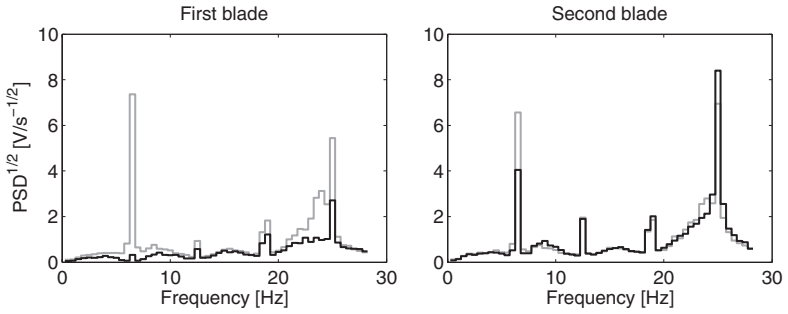

Figure 11. Load PSD with (black) and without (grey) SISO feedback control at 0° yaw.

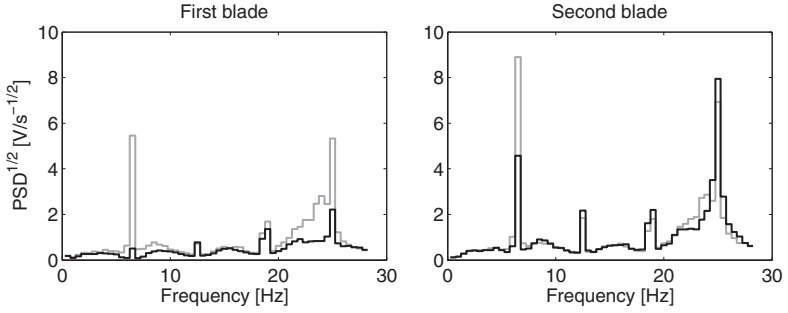

Figure 12. Load PSD with (black) and without (grey) SISO feedback control at 5° yaw.

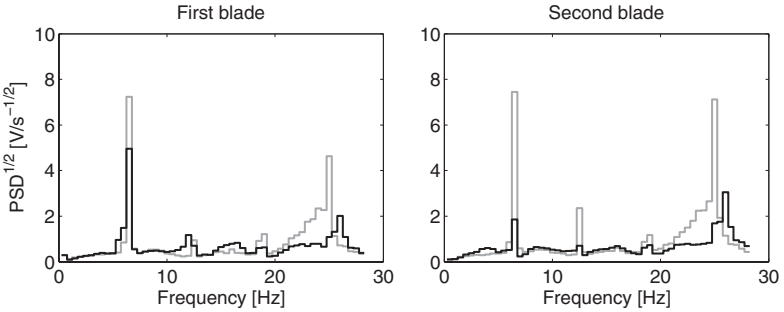

Figure 13. Load PSD with (black) and without (grey) MIMO feedback control at 0° yaw.

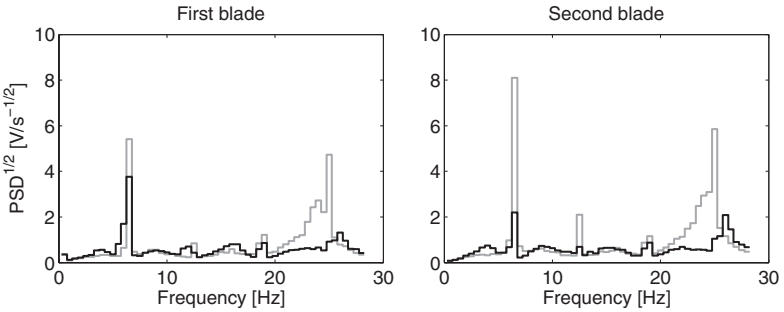

Figure 14. Load PSD with (black) and without (grey) MIMO feedback control at 5° yaw.

amplification of the 4P spike because of the interaction with the first bending mode can be observed. Comparing both figures, one would have expected a higher induced loading for the 5° yaw load case, but this is not the case. The exact reason for this is yet to be determined, but it could be that in the 0° load case the induced disturbances were so large that the added effect of a small yaw angle posed only little additional loads. Also, a difference of the behaviour of blade 1 and 2 can be observed. We believe that this could be attributed to small differences in blade manufacturing and a slight unbalance of the rotor. Regarding the performance of the SISO controller, we can conclude from the figures that the SISO controller failed to add damping to the first mode for blade 2.

However, the controllers on the two blades were acting independently, even though the action of each controller had a large effect on the response of the other blade, because of the high degree of coupling present in the system. Therefore, with parallel SISO control, the controllers might have been working against each other.

4.2. MIMO control

As a result of these issues that were encountered with SISO control, MIMO control was implemented; the results of which can be seen in Figures 13 and 14. The same load spectrum (without controller) as with the SISO controller was observed and the 5° yaw load case posed no significantly different spectrum. The load reduction was much higher than with parallel SISO control and it maintained high load reduction at a 5° yaw angle for both blades. In particular, the blade dynamics were damped much better, at the expense of the reduction of the 1P loads.

4.3. Combined MIMO and RC control

Subsequently, a combination of the MIMO feedback controller with a feedforward controller was tested (see Figures 15 and 16). As can be observed comparing Figures 13 and 14 to Figures 15 and 16, a better performance regarding the 1P loads was attained. For this controller, two time series plots for blade 1 are also presented (see Figure 17) for 0° and for 5° yaw.

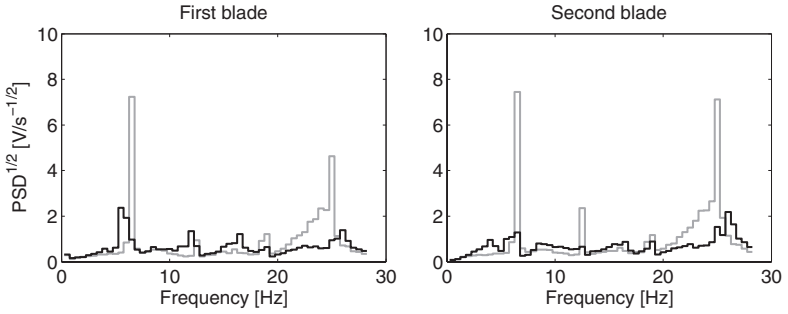

Figure 15. Load PSD with (black) and without (grey) feedforward and MIMO control at 0° yaw.

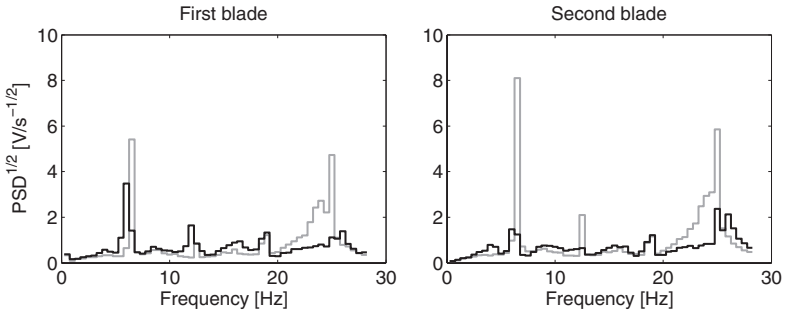

Figure 16. Load PSD with (black) and without (grey) feedforward and MIMO control at 5° yaw.

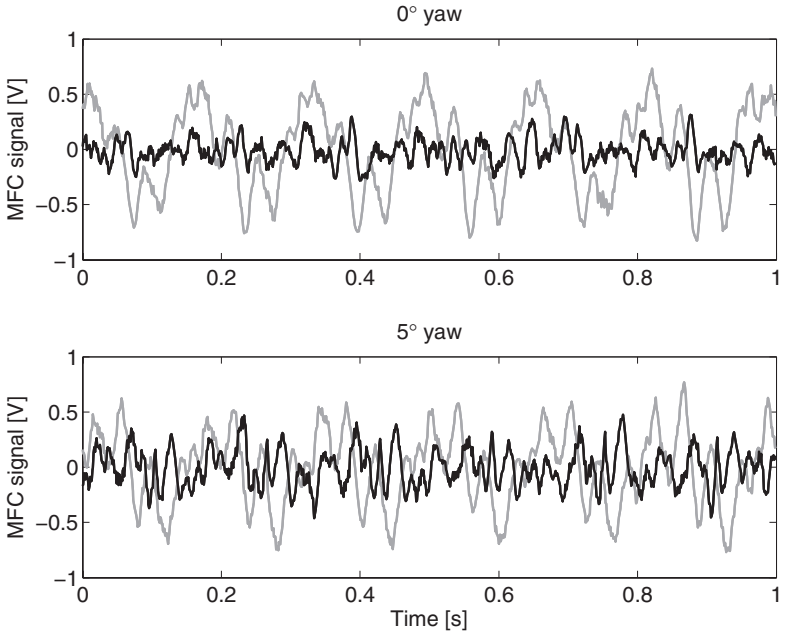

Figure 17. Time series of blade 1 with feedforward and MIMO control for two yaw cases.

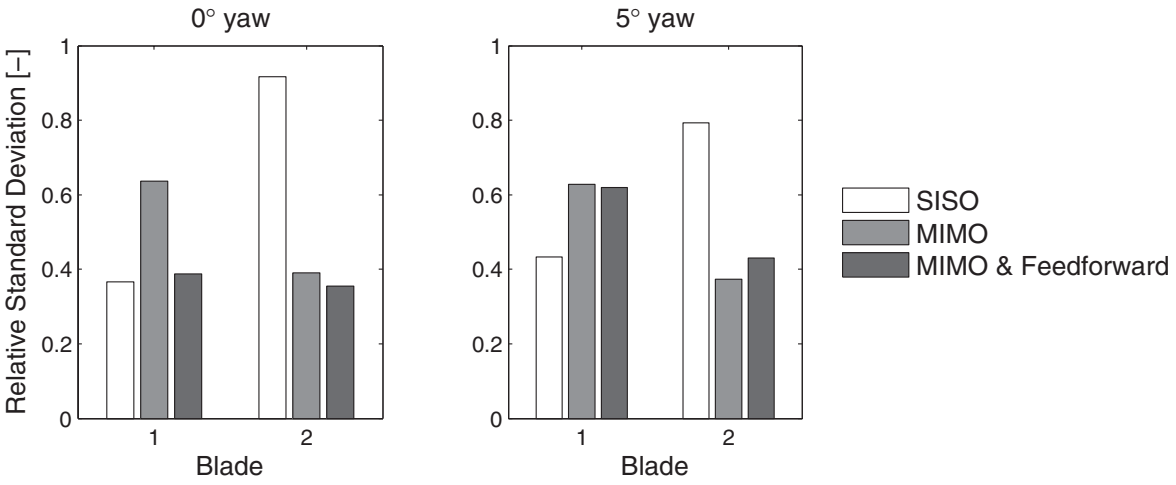

Figure 18. Standard deviation, relative to the corresponding uncontrolled load case for the different controllers.

In these figures, the same observed behaviour as in the PSD figures can be seen. The 1P load with a period of about 0.16 s was greatly reduced, especially for the zero yaw case, but there was a penalty to be paid in the form of high frequency disturbances. The same holds for the 5° yaw load case, although there seemed to be a high frequency component which was less mitigated.

4.4. Controller comparison

Finally, we present the standard deviation of the MFC signal, relative to the same load case without any controller. Thus, a value of 1 equals the standard deviation for the respective load case without a controller:

$$\text{Rel. standard deviation} = \frac{\text{std}(\text{MFC}_{\text{with control}})}{\text{std}(\text{MFC}_{\text{without control}})} \tag{5}$$

Where std(MFC) is the standard deviation of a captured time series of the MFC signal. This provides a good estimation of the reduction in dynamic loads (see Figure 18). The SISO controller obviously worked well for blade 1, but hardly any reduction was seen for blade 2. This was also consistent with the PSDs in Figures 11 and 12 and it was because the gains of the controller were tuned for blade 1 first. This way a good controller for blade 2 was hard to obtain. The MIMO controllers with and without feedforward control showed similar results, although the one with feedforward control at 1P seemed to perform slightly better in total standard deviation reduction.

5. SUMMARY AND FUTURE WORK

In this paper, we discussed the design procedure for a smart rotor, equipped with variable trailing-edge geometry. The dynamic behaviour of the blades was analysed, also with sensor selection and placement in mind. Different controllers were designed, based on the measured behaviour of the system. Both feedback and feedforward controllers were based on the structural response of the blade to dynamic loading.

The rotor was tested under different yaw conditions with the different controllers. In general, significant reductions of the dynamic amplitude were attained with all controllers. The SISO feedback control gave some load reduction, but mainly for the blade to which the controller gains were tuned first. The MIMO controller gave better performance, but the performance at 1P was slightly increased when an adaptive feedforward controller, aimed at the 1P loads, was added. However, some penalty was paid for reducing loads at the multiple-P and around the first natural frequency of the blade by a slight increase in loads in other parts of the spectrum. In general, the results showed that a large dynamic load reduction is attainable, but that the coupling between the different blades on a rotor has to be taken into account in controller design.

Thus, through presenting a design procedure for—and experiments on—a smart rotor this research provided a framework for successful implementation of load control to a rotor. However, for implementation on a full scale turbine

DOI: 10.1002/we

several topics are still to be addressed, such as the design of the flaps on that scale and the reliability and stability of the system.

In the future, load cases other than operating the scaled rotor in yaw will be tested. Also, different controllers will be developed to target the different deterministic and stochastic loads. Increasing the flap authority through a better actuator shape and greater deflection could greatly increase the load reduction potential of the system. In addition, analyses of the turbine through aero-elastic modelling are planned.

ACKNOWLEDGMENTS

This research was supported by the European Commission's UpWind program and the Dutch Technology Foundation STW and performed within the Delft University of Technology's wind energy research institute DUWIND.

REFERENCES

1. Griffin DA. Windpact turbine design scaling studies technical area 1 composite blades for 80- to 120-meter rotor. *Technical Report SR-500–29492*, National Renewable Energy Laboratory: Golden, CO, 2001.
2. Brøndsted P, Lilholt H, Lystrup A. Composite materials for wind power turbine blades. *Annual Review of Materials Research* 2005; **35**: 505–538.
3. Hansen AD, Hansen LH. Wind turbine concept market penetration over 10 years (1995–2004). *Wind Energy* 2007; **10**: 81–97.
4. Bianchi FD, De Battista H, Mantz RJ. (eds). *Wind Turbine Control Systems—Principles, Modelling and Gain Scheduling Design*. Springer: London, UK, 2007.
5. Selvam K, Kanev S, van Wingerden JW, van Engelen T, Verhaegen M. Feedback-feedforward individual pitch control for wind turbine load reduction. *International Journal of Robust and Nonlinear Control, special issue on Wind turbines: New challenges and advanced control solutions* 2008; **19**: 72–91.
6. Larsen TJ, Madsen HA, Thomsen K. Active load reduction using individual pitch, based on local blade flow measurements. *Wind Energy* 2005; **8**: 67–80.
7. Bossanyi EA. Individual blade pitch control for load reduction. *Wind Energy* 2003; **6**: 119–128.
8. de Goeij WC, van Tooren MJL, Beukers A. Implementation of bending-torsion coupling in the design of a wind-turbine rotor-blade. *Applied Energy* 1999; **63**: 191–207.
9. Lobitz DW, Veers PS, Eisler GR, Laino DJ, Migliore PG, Bir G. The use of twist-coupled blades to enhance the performance of horizontal axis wind turbines. *Technical Report SNAD2001-1303*, Sandia, 2001.
10. Lobitz DW, Laino DJ. Load mitigation with twist-coupled HAWT blades. In *Proceedings of the ASME Wind Energy Symposium*, January 1999.
11. Barlas T. van Kuik GAM. Review of state of the art in smart rotor control research for wind turbines. *Progress in Aerospace Sciences* 2010; **46**: 1–27.
12. Standish KJ, van Dam CP. Computational analysis of a microtabbased aerodynamic load control system for rotor blades. *Journal of the American Helicopter Society* 2005; **50**: 249–258.
13. Mayda EA, van Dam CP, Yen Nakafuji D. Computational investigation of finite width microtabs for aerodynamic load control. *Proceedings of the 43rd AIAA Aerospace Science Meeting and Exhibit*, January 2005.
14. Basualdo S. Load alleviation on wind turbine blades using variable airfoil geometry. *Wind Engineering* 2005; **29**: 169–182.
15. Buhl T, Gaunaa M, Bak C. Potential load reduction using airfoils with variable trailing edge geometry. *Journal of Solar Engineering* 2005; **127**: 503–516.
16. Joncas S, Bergsma O, Beukers A. Power regulation and optimization of offshore wind turbines through trailing edge flap control. *Proceedings of the 43rd AIAA Aerospace Science Meeting and Exhibit*, January 2005.
17. Rice JK, Verhaegen M. Robust and distributed control of a smart blade. *Wind Energy* 2010; **13**: 103–116.
18. Andersen PB, Gaunaa M, Bak C, Buhl T. Load alleviation on wind turbine blades using variable airfoil geometry. *Proceedings of the European Wind Energy Conference and Exhibition*. European Wind Energy Association, Brussels, 2006.
19. Andersen PB, Henriksen L, Gaunaa M, Bak C, Buhl T. Deformable trailing edge flaps for modern megawatt wind turbine controllers using strain gauge sensors. *Wind Energy* 2010; **13**: 193–206.

20. Bak C, Gaunaa M, Andersen PB, Buhl T, Hansen P, Clemmensen K, Moeller R. Wind tunnel test on wind turbine airfoil with adaptive trailing edge geometry. *Proceedings of the 45th AIAA Aerospace Science Meeting and Exhibit*, January 2007.
21. van Wingerden JW, Hulskamp AW, Barlas T, Marrant B, van Kuik GAM, Molenaar DP, Verhaegen M. On the proof of concept of a 'smart wind turbine rotor blade for load alleviation. *Wind Energy* 2008; **11**: 265–280.
22. Hulskamp AW, Beukers A, Bersee HEN, van Wingerden JW, Barlas T, van Kuik GAM. Design of a wind tunnel scale model of an adaptive wind turbine blade for active aerodynamic load control experiments. *Proceedings of the 16th International Conference of Composite Materials*, July 2007.
23. XFOIL [Online]. Available: http://raphael.mit.edu/xfoil/.website (Accessed 26 July 2010).
24. Du Z, Selig MS. A 3D stall-delay model for horizontal axis wind turbine performance prediction. *Proceedings of the 36th AIAA, Aerospace Sciences Meeting and Exhibit and 1998 ASME Wind Energy Symposium*, January 1998.
25. van Rijswijk K. Thermoplastic composite wind turbine blades: vacuum infusion technology for anionic polyamide-6 composites. PhD Thesis, Delft University of Technology, 2007.
26. Fagerberg L. Wrinkling and compression failure transition in sandwich panels. *Journal of Sandwich Structures and Materials* 2004; **6**: 129–144.
27. Aimmannee S, Hyer MW. Analysis of the manufactured shape of rectangular THUNDER-type actuators. *Smart Materials and Structures* 2004; **13**: 1389–1406.
28. Sessler GM. Piezoelectricity in polyvinylidenefluoride. *Journal of the Acoustical Society of America* 1981; **70**: 1596–1608.
29. Sodano HA, Park G, Inman DJ. An investigation into the performance of macro-fiber composites for sensing and structural vibration applications. *Mechanical Systems and Signal Processing* 2004; **18**: 683–697.
30. Open Jet Facility [Online]. Available: http://www.lr.tudelft.nl/live/pagina.jsp?id=264683f6-4e46-4b40-8d9f-b47d2577c073&lang=en (Accessed 26 July 2010).
31. Verhaegen M, Verdult V. *Filtering and System Identification: A Least Squares Approach*. Cambridge University Press: Cambridge, 2007.
32. van der Meulen S, Tousain RL, Bosgra OH. Fixed structure feedforward controller design exploiting iterative trials: Application to a wafer stage and a desktop printer. *Journal of Dynamic Systems, Measurement, and Control* 2008; **130**: 051006.